Evaluation of the dissolution behavior of zircon using high-resolution phase-shift interferometry microscope

Toru KITAGAKI[a]*

[a] *Collaborative Laboratories for advanced Decommissioning Science, Japan Atomic Energy Agency, Tokai-mura, Japan*

Address: 2-4 Shirakata, Tokai-mura, Ibaraki, Japan 319-1195, Tel: 029-282-6810, email: kitagaki.toru@jaea.go.jp

Abstract

The dissolution behavior of the (101) plane of zircon mineral in ultrapure water, 1 M HCl (aq), and 1 M NaOH (aq), under room temperature and nearly atmospheric pressure was evaluated by in situ measurement of the change in the surface height. A high-resolution phase-shift interferometry microscope (HR-PSI) was employed to evaluate the velocity of the change in the surface height of zircon in different solutions, and the application of this method in evaluating the dissolution behavior of nuclear materials was examined. In all cases, the measured surface height decreased linearly with small variations. Although the measured change in height of zircon in 1 M NaOH (aq) was the smallest under these conditions, the concentration of dissolved Zr in NaOH (aq) was two orders of magnitude higher than that in ultrapure water. This indicates that a high amount of dissolved Zr in 1 M NaOH (aq) was immediately precipitated on the zircon surface as a secondary phase, and the surface shape was almost retained. On the other hand, the precipitation on the reference of the surface height was confirmed while measuring the zircon in 1 M HCl (aq). This shows that the precipitation in 1 M HCl (aq) occurred far from the dissolution points, and the surface shape changed. As a result, the velocity of surface change and the precipitation behavior of zircon, which is one of the extremely durable minerals, was successfully evaluated using HR-PSI. This relatively quick method would be useful for evaluating the detailed surface change behaviors of nuclear materials, such as fuel debris, ceramic waste forms, and UO_2, during the reaction with various solutions, since it minimises radiation exposure times and also the amount of radioactive waste generation during measurement.

Keywords: zircon; in situ measurement; dissolution; phase-shift interferometry; fuel debris; mineral

1. Introduction

Mineral–water interactions, such as dissolution of minerals and precipitation of the dissolved elements, play a significant role in geological element cycles [1]. The buried or Earth-based artificial materials are gradually dissolved in water, and the dissolved elements migrate to the geological environment with other elements. In nuclear waste disposal, radionuclides are released when the vitrified radioactive waste or spent nuclear fuels are dissolved in geological depositories. In the case of post-severe accidents, such as the three-mile Island unit 2 (TMI-2), Chernobyl nuclear power plant unit 4 (ChNPP), and Fukushima Daiichi nuclear power plants (1F), fuel debris, which are fuel-containing materials produced as a result of the melting of the reactor core, were generated, and parts of them were dissolved in the surrounding water [2-4]. Radionuclides are hazardous to humans; therefore, their dissolution should be investigated for risk evaluation of radiation, nuclear fuel material control, and so on. Several dissolution experiments using actual- or simulant-vitrified radioactive waste, nuclear fuels, or fuel debris have been conducted to examine their dissolution in water [5-14]. In these studies, the dissolution behavior were evaluated mainly by measuring the change in the elemental concentration of the solutions with time. The vitrified radioactive waste and UO_2 in spent nuclear fuels are homogeneous on a macroscopic scale, and the dissolution from their surface is almost homogeneous. Therefore, the estimated dissolution behavior, such as the dissolution rate of the elements from the measurement results, are considered reasonable. On the other hand, fuel debris has multiple phases, and the microstructure is heterogeneous [15, 16]. Therefore, the dissolution behavior of fuel debris must always be different. Thus, it is difficult to evaluate the dissolution of fuel debris by measuring the elemental concentration of the solutions.

Recently, high vertical resolution microscopes, including atomic force microscope (AFM), and white light interferometers, such as vertical scanning interferometer (VSI) and phase-shift interferometer (PSI), have been used to evaluate the interaction of mineral water interface [1]. Near-neutral water properties are appropriate for AFM measurements to avoid damage to the device as AFM is a contact observation method. On the other hand, PSI is a noncontact observation method and can be used for in-site measurements, regardless of the properties of the solution, such as pressure, temperature, acidity, and basicity [17]. To evaluate the dissolution behavior of fuel debris, dipping in various solutions, such as seawater, alkaline, boric, and acids solution, should be considered [3, 4]. Therefore, it seems that PSI is appropriate for evaluating the dissolution behavior of fuel debris in various solutions.

In the case of the TMI-2 accident, $(U,Zr)O_2$ and other phases were produced by in-vessel high-temperature reactions of the core materials, such as UO_2, zircalloy, and stainless steel [15]. On the other hand, in the case of the ChNPP accident, molten fuel-containing materials reacted with concrete or concrete-like materials [16]. Various fuel debris with amorphous SiO_2 matrix was

produced, and various phases, such as $(Zr,U)SiO_4$, UO_2, and $(U,Zr)O_2$, were precipitated in the matrix, and various elements, such as Al, Mg, Ca, Zr, and U, were dissolved in the matrix [16, 18-25]. In the case of the 1F accident, a part of the molten reactor core reacted with concrete [26]. Therefore, the formation of similar chemical phases as those of the fuel debris in ChNPP was predicted [27]. Zircon is one of the most chemically stable phases in fuel debris owing to its extreme durability [28]. Therefore, the change in surface height due to the reaction with solutions would be smaller than that of other phases. If the change in the surface height of zircon can be measured by PSI, that of other phases in the fuel debris can also be measured by the same technique.

Zircon is an important mineral for estimating ancient geological environments owing to its chemical stability [29]. It is also a good candidate for the host phase to immobilize weapon-grade Pu [19, 30-35]. Thus, its dissolution under high temperature and/or high pressure simulating the geological environments has been evaluated [36-39], but the dissolution under room temperature and atmospheric pressure is rarely evaluated owing to the chemical durability [36].

Here, we evaluated the dissolution of zircon ($ZrSiO_4$) in strong acid, 1 N HCl (aq), base, 1 N NaOH (aq), and ultrapure water under room temperature and near-atmospheric pressure using high-resolution PSI (HR-PSI) and discuss the applicability of the method in evaluating the dissolution behaviors of nuclear materials, such as fuel debris, ceramic waste forms and UO_2.

2. Methods

2.1. High-resolution phase shift interferometry

HR-PSI, developed by H. Satoh et al. [17], was employed in this study. Its detailed structure and performance can be found in [17, 40, 41]. It achieves in situ measurement of the growth/dissolution rate of various materials in liquid down to the order of 10^{-5} nm/s [17].

Here, the specimen for in situ measurements was fixed by gold wire on the holder made of polyether ether ketone in the in situ observation cell, Syn-corporation PC20-200. The solutions to flow in the cell were ultrapure water, 1 M HCl (aq), and 1 M NaOH (aq). The refractive index of each solution at 25 ℃ (n_{25}) was measured using an abbe refractometer, and the results are listed in Table 1. The solution was pumped by a high-performance liquid chromatography plunger pump at 0.5 MPa, from 11.6 to 42.8 μL/min, and was heated in the cell at 25 ± 0.1 ℃. It then flowed into the in situ observation cell. The drainage was injected in a sealed centrifuge tube, and the concentrations of Zr and Si in the solutions dissolved from zircon were measured by inductively coupled plasma mass spectrometry (ICP-MS).

The initial surface of the zircon (101) plane was observed by HR-PSI, and the interference image of the zircon surface captured every 30 s are shown in Figure S1 and S2 in the Supplementary materials, respectively.

2.2. Materials

Zircon from Sri Lanka [42] (Figure 1) was used in the experiment. The property of the zircon is shown in Table 2. The piece of zircon with the (101) plane was set on the in situ observation cell, as shown in Figure 2.

The change in height on the (101) plane of the zircon during the reaction with the solution was measured using HR-PSI. The reference point of the height is needed to measure the changes in height. Gold (111) small crystals, which are insoluble, were used as the reference. They were dispersed in the ultrapure water containing the zircon specimen, and an adhered crystal on the (101) plane of zircon was used as the reference point.

The surface area, SA (m^2) of the zircon specimen that contacts with the solution, except for the bottom, was estimated from the SA in Figure 2, and it was 5.114×10^{-6} m^2.

2.3. Height change velocity

The velocity of change in height, V_{height} (nm/s), with the surface height change measured by HR-PSI was evaluated as the slope of the linear approximation by least squares method of the measured height change. The (101) surface height of zircon was measured every 30 s as mentioned above.

2.4. Dissolution rate

The dissolution rate, *Rate* (mol/m^2/s), with the measured Zr and Si concentrations in the solution, $C_{Zr\ or\ Si}$ (mol/L), was calculated using Equation (1), as shown below.

$$Rate = \frac{F \times (C_{Zr\ or\ Si,out} - C_{Zr\ or\ Si,in})}{SA \times n_{Zr\ or\ Si}}, \qquad (1)$$

where subscripts "in" and "out" indicate the inlet and outlet of the solution to the in situ observation cell, respectively. F is the flow rate (L/s), $n_{Zr\ or\ Si}$ is the stoichiometric coefficient of the zircon dissolution reaction. In this case, n_{Zr} and n_{si} are 1.

3. Results

3.1. Velocities of height change measured by HR-PSI

The initial height profiles of the zircon surface at two lines, L100 and L350, are shown in Figure 3. The region of L100 is continuously inclined and that of L350 crosses the growth hill. The signs of the circles on the lines indicate the measurement points for the height changes while flowing ultrapure water. The position of the two lines on the phase image of the zircon surface observed by HR-PSI is shown in Figure S1 of the Supplementary materials. The height in the phase image is represented by 255 tones from black to white in each $532/2n_{25}$ nm. The n_{25} of each solution is

shown in Table 1. The sign of Au in the phase image is the height reference used in the height measurement.

The time-line images of L100 and L350 while flowing ultrapure water were obtained by HR-PSI and are shown in Figure S2. The height changes for each point on the lines extracted from the timeline images are shown in Figure S3 and S4. The V_{height} of each point was calculated from the slope of the linear approximation by least squares method of the height changes and is shown in Figure 4. The height of all points gradually decreased from the initial points. This means that the dissolution is the dominant reaction compared to precipitation. The height at higher positions decreased more than that at lower positions. This could be for two reasons: the effect of the water flow conditions, such as speed, meandering, and vortex; the variation in the ease of dissolution due to the slope of the surface. The effect of the water flow is minimal because the differences in the height on the lines are small. The step of the crystal surface decreases in the horizontal direction during the dissolution [43]. Therefore, a sharp slope has dense steps and the apparent velocity of the decrease in height on the sharp slope during dissolution is large. The correlation between the slope of the vicinal surface and the V_{height} is shown in Figure 5. The degree of slope of each point is expressed as follows:

$$\tan\theta = \frac{d}{\lambda},$$

where d is the height of steps and λ is the interstep distance. The V_{height} change with a steeper slope is larger than that of the gradual-slope region. This tendency is opposite to that in the dissolution of calcite [41, 44] and anorthite [17]. It implies that precipitation occurred at each step and apparent velocity decreased. This is discussed in detail in a later section.

The average dissolution rates in L100 and L350 are -1.55×10^{-4} and -1.39×10^{-4} nm/s, respectively (Figure 6). These values are reasonable as they are within the performance of the resolution of the height measurement by HR-PSI (order of 10^{-5} nm/s).

V_{height} while flowing HCl (aq) and NaOH (aq) was also measured with the same procedure. The phase images before the measurements, the timeline images, and the measured V_{height} are shown in Figure S5–S15. The measured V_{height} while flowing HCl (aq) and NaOH (aq) is shown in Figure 6. In the case of HCl (aq), the deviations of the values are larger than those of other cases. It seems that the deviation stems from the precipitation on the reference surface. Figure S7 shows the fluctuation of the surface while flowing HCl (aq). The V_{height} while flowing NaOH (aq) was the lowest. This does not imply poor dissolution of zircon in NaOH (aq), rather it implies that the dissolution and precipitation reactions are comparable, as discussed in detail in a later section. The deviation of the measurements between different lines under the same condition was small. It shows that the reactions of the zircon with the solutions are homogeneous, and the resolutions of the height measurements by HR-PSI can be applied to measure V_{height} of chemically durable minerals, including zircon.

3.2. Dissolution of Si and Zr measured by ICP-MS

The measured changes in the concentrations of Zr and Si in each solution are shown in Figures 7 and 8, respectively. The concentration of Zr while flowing ultrapure water or HCl (aq) in figure 7, and that of Si while flowing ultrapure water in figure 8 were close to the detection limit. The concentrations of the dissolved elements were almost constant while flowing the same solutions. This is similar to the changes in surface height measured by HR-PSI. The dissolution rates were calculated from each measured concentration, as shown in Figure 9. In all cases, the dissolution rates of Si were more than one order of magnitude larger than that of Zr. It means that the dissolution of zircon is incongruent under wide pH range in HCl (aq) and NaOH (aq) conditions. We infer that most dissolved Zr and Si from the zircon surface immediately precipitated on the dissolved surface. The dissolution rate of Si while flowing NaOH (aq) was much higher than that while flowing ultrapure water but close to that while flowing HCl (aq). This is different from the results of the surface V_{height}. The reason for this variation is discussed later.

3.3. The surface observation by atomic force microscopy

The (101) surface of zircon after the measurement by PSI was observed by AFM (Veeco Demension 3100 AFM), as shown in Figure 10. It reveals several protruding objects, suggesting that NaOH that was precipitated on the surface of the specimen because of the drying of NaOH (aq). Etch pits are also observed as indents on the surface, and small sediments are shown in the etch pit. The shape of the sediments is classified into two: sheet-like materials (ppt-A) and particle-like materials (ppt-B). The detailed characteristics, including elemental composition and chemical phase, are unknown. Nevertheless, it is evidence that precipitation reaction occurred immediately after the dissolution of zircon.

4. Discussion

4.1. Zircon dissolution behavior

The dissolution behavior of Zr and Si in each solution are to be expected as below. The dissolution rate of Si was more than one order of magnitude higher than that of Zr under the considered experimental conditions, as shown in Figure 9. The variations in the height change of the zircon surface in ultrapure water and NaOH (aq) were small compared to those of zircon in HCl (aq). This is because zircon in ultrapure water and NaOH (aq) forms etch pits on the crystal surface, and most Zr immediately precipitates in the etch pits or near the surface. On the other hand, precipitation on the reference Au nanocrystal was confirmed during the in situ measurement of the zircon surface in HCl (aq). We infer that the Zr dissolved in HCl (aq) precipitated far from the etch pits. Although a portion of Si should also be precipitated with Zr, the characteristics of the precipitation are unknown.

The surface modification of the zircon is explained as below. The changes in surface height and the concentration of dissolved Zr and Si in ultrapure water and NaOH (aq) were almost constant in the duration of the experiments (several days). This is because that the dissolution of zircon measured was the initial stage of zircon dissolution. The dissolution of zircon, which means $ZrSiO_4$ crystal units departing from the steps of the crystal surface [43], occurs in the unreacted surface, then other dissolution starts from the other unreacted area, and that is how the reacted area on the zircon surface gradually spreads. Figure 10 shows that there were many unreacted areas.

While flowing ultrapure water, the surface V_{height} was slower than that of other conditions. Generally, the dissolution of crystals proceeds by retreating the steps in a horizontal direction [43]. Therefore, a decrease in height in the region with dense steps is higher than that in the nondense regions, such as calcite [41, 44] and anorthite [17]. On the other hand, V_{height} of zircon decreases with an increase in the slope of the surface. This is similar to the dissolution accompanied by precipitation, such as olivine [45]. The precipitate accumulates between the steps, and the apparent V_{hight} decreases. Therefore, it is difficult to convert the measured V_{height} to the retreat velocity of the step, which is the physically accurate crystal dissolution velocity.

While flowing HCl (aq), the vibrations of the height change were larger than those of other conditions because of the frequent precipitation on the surface of the reference. Moreover, the concentrations of Zr and Si in HCl (aq) were also higher than that in other conditions. Therefore, the rates of dissolution and precipitation are higher than those in other conditions.

While flowing NaOH (aq), although V_{height} was the slowest, the dissolved Si in the solution was equivalent to that in HCl (aq), and the dissolved Zr was equivalent to that in ultrapure water. This shows that most dissolved Zr immediately precipitated on the dissolved surface.

From these results, we infer that the surface structure of zircon after dipping in different solutions shows various surface modifications because of the dissolution and precipitation behaviors, depending on the properties of the solutions. Therefore, an evaluation of the detailed surface modification of zircon would be useful to better understand the dissolution and precipitation behaviors of zircon.

4.2. Applications to evaluate dissolution behaviors of nuclear materials

Severe accidents of nuclear reactors cause high-temperature reactions of nuclear fuels, e.g. UO_2 and PuO_2, with the structural materials, such as SUS, Zr, and concrete under various atmospheric conditions with moisture [46, 47].. The reaction products of these components are multiphase and heterogeneous materials [16, 48, 49] called fuel debris. The main phases of fuel debris generated in TMI-2 are UO_2, $(U,Zr)O_2$, and U–Zr–O [48, 49]. $(Zr,U)SiO_4$ was also confirmed in the fuel debris of ChNPP [16]. $(Zr,U)SiO_4$ is similar to zircon, but it contains a higher concentration of uranium than natural zircon. Zircon is one of the most chemically stable minerals and one of the

minerals with the lowest dissolution rate [28]. Therefore, if V_{height} of zircon can be measured, that of the other phases can also be measured. In this study, V_{height} of the zircon was successfully measured. Since PSI can only be used for observation, there is a need to identify the phase distribution and secondary phases formed by the reactions in different solutions, to understand the dissolution behavior. The phase distribution and secondary phases in fuel debris can be identified before and after in situ measurements of V_{height}. The spatial resolution of HR-PSI is several micrometers. Therefore, it is necessary to identify the position of small phases, less than several micrometers. Moreover, measuring the dissolved elements in the solutions is necessary to evaluate the precipitation behavior.

The remarkable advantages of employing in situ measurements of the surface V_{height} by HR-PSI in evaluating the dissolution of fuel debris include the decrease in radiation exposure time and radioactive wastewater during measurement because of the short measurement time and use of a small amount of solution. The same solutions in which fuel debris is actually dipped into are used to evaluate the accurate dissolution behavior of fuel debris in the actual environment.

Using this in situ measurement to evaluate the dissolution behavior of ceramic waste forms for actinide immobilization and UO_2 dissolution for direct disposal is also useful. The knowledge of the kinetic surface change behavior of UO_2 in solutions is limited. Therefore, employing the method to evaluate the kinetics of UO_2 dissolution gives a deep knowledge to understand the surface modification of UO_2 in various solutions. When UO_2 is dipped in the solutions, the dissolved $U(VI)O_2^{2+}$ precipitates on the surface as secondary phases, such as Shoepite, $UO_3 \cdot nH_2O$, and Dehydrated Schoepite, $UO_3 \cdot (0.8–1.0\ H_2O)$ [50]. Therefore, we infer that the trend of V_{height} is similar to that of zircon. In addition, in situ measurements of the change in the height of spent nuclear fuel in nitric acid to evaluate the dissolution behavior for aqueous reprocessing, such as the PUREX process, can be employed to optimize the dissolution process and understand the dissolution behavior of spent nuclear fuels in detail.

5. Conclusion

The V_{height} of the (101) plane of zircon, which is one of the most chemically stable minerals, in ultrapure water, 1 M HCl (aq), and 1 M NaOH (aq) was successfully obtained by in situ measurements of the surface height changes using HR-PSI. Moreover, the knowledge of the dissolution and precipitation behaviors of the zircon was obtained from detailed in situ measurements of the surface height changes by HR-PSI, and the measurement of Zr and Si concentrations in each solution by ICP-MS. In the case of evaluating the dissolution behavior along with precipitation, phase identification and concentration measurement of the elements in the solutions are needed. This method is useful for evaluating the kinetic surface modification in detail during the dissolution of nuclear materials, such as fuel debris and UO_2. It is also useful

when considering the decrease in radiation exposure time and amount of radioactive waste during the measurement.

4

Acknowledgments

This work was supported by JSPS KAKENHI Grant Number JP16671777, JP21428140. I thank Hisao SATOH (Mitsubishi materials) for the great contribution in the in situ measurement using HR-PSI.

References

[1] C.V. Putnis, E. Ruiz-Agudo, The mineral-water interface: Where minerals react with the environment, Elements 9(3) (2013) 177-182.
[2] W.C. Holton, C.A. Negin, S.L. Owrutsky, The cleanup of Three Mile Island unit 2, Electric Power Research Institution, 1990.
[3] O.O. Odintsov, E.V. Khan, O.V. Krasnov, M.V. Shcherbin, Long-term monitoring of the unorganized accumulations liquid radioactive wasters of object «Ukryttya», Problems of Nuclear Power Plants' Safety and of Chornoby (27) (2016) 43-57.
[4] Fukushima Daiichi radwaste analytical data library. https://frandli-db.jaea.go.jp/FRAnDLi/index.php?country=e. (Accessed November 25 2020).
[5] A. Banos, T.B. Scott, A review of the reaction rates of uranium corrosion in water, Jounal of Hazardous Materials 399 (2020) 122763.
[6] A. Nakayoshi, C. Jegou, L. De Windt, S. Perrin, T. Washiya, Leaching behavior of prototypical corium samples: A step to understand the interactions between the fuel debris and water at the Fukushima Daiichi reactors, Nuclear Engineering and Design 360 (2020).
[7] Y. Kumagai, M. Takano, M. Watanabe, Reaction of hydrogen peroxide with uranium zirconium oxide solid solution - zirconium hinders oxidative uranium dissolution, Journal of Nuclear Materials 497 (2017) 54-59.
[8] S.T. Barlow, D.J. Bailey, A.J. Fisher, M.C. Stennett, C. Gausse, H. Ding, V.A. Krasnov, S.Y. Sayenko, N.C. Hyatt, C.L. Corkhill, Synthesis, characterisation and corrosion behaviour of simulant Chernobyl nuclear meltdown materials, npj Materials Degradation 4(1) (2020).
[9] T. Sasaki, Y. Takeno, T. Kobayashi, A. Kirishima, N. Sato, Leaching behavior of gamma-emitting fission products and Np from neutron-irradiated UO_2–ZrO_2 solid solutions in non-filtered surface seawater, Journal of Nuclear Science and Technology 53(3) (2015) 303-311.
[10] S. Gin, A. Abdelouas, L.J. Criscenti, W.L. Ebert, K. Ferrand, T. Geisler, M.T. Harrison, Y. Inagaki, S. Mitsui, K.T. Mueller, J.C. Marra, C.G. Pantano, E.M. Pierce, J.V. Ryan, J.M. Schofield, C.I. Steefel, J.D. Vienna, An international initiative on long-term behavior of high-level nuclear waste glass, Materials Today 16(6) (2013) 243-248.
[11] D.W. Shoesmith, Fuel corrosion processes under waste disposal conditions, Journal of Nuclear Materials 282 (2000) 1-31.
[12] B. Zubekhina, B. Burakov, E. Silanteva, Y. Petrov, V. Yapaskurt, D. Danilovich, Long-term aging of Chernobyl fuel debris: Corium and “lava”, Sustainability 13(3) (2021).
[13] B.Y. Zubekhina, B.E. Burakov, Leaching of actinides and other radionuclides from matrices of Chernobyl “lava” as analogues of vitrified HLW, The Journal of Chemical Thermodynamics 114 (2017) 25-29.
[14] B.Y. Zubekhina, B.E. Burakov, O.G. Bogdanova, Y.Y. Petrov, Leaching of ^{137}Cs from Chernobyl fuel debris: corium and “lava”, Radiochimica Acta 107(12) (2019) 1155-1160.
[15] R.K. Mccardell, M.L. Russel, D.W. Akers, C.S. Olsen, Summary of TMI-2 core sample examination, Nuclear Engineering and Design 118 (1990) 441-449.
[16] É.M. Pazukhin, Fuel-containing lavas of the Chernobyl NPP fourth block: Topography, physicochemical properties, and formation scenario, Radiochemistry 36(2) (1994) 109-154.
[17] H. Satoh, Y. Nishimura, K. Tsukamoto, A. Ueda, K. Kato, S. Ueta, In-situ measurement of dissolution of anorthite in Na-Cl-OH solutions at 22°C using phase-shift interferometry, American Mineralogist 92(4) (2007) 503-509.

[18] E.B. Anderson, B.E. Burakov, E.M. Pazukhin, High-uranium zircon from "Chernobyl lavas", Radiochimica Acta 60 (1993) 149-151.
[19] B.E. Burakov, A study of high-uranium technologenous zircon (Zr,U)SiO_4 from Chernobyl "lavas" in connection with the problem of creating a crystalline matrix for high-level waste disposal, International Conference Safewaste 93, Avignon, France, 1993, pp. 19-28.
[20] B.E. Burakov, E.B. Anderson, B.Y. Galkin, E.M. Pazukhin, S.I. Shabalev, Study of Chernobyl hot particles and fuel containing masses: Implication for reconstructing the initial phase of the accident, Radiochimica Acta 65 (1994) 199-202.
[21] T. Geisler, B.E. Burakov, V. Zirlin, L. Nikolaeva, P. Pöml, A Raman spectroscopic study of high-uranium zircon from the Chernobyl "lava", European Journal of Mineralogy 17(6) (2006) 883-894.
[22] P. Pöml, B. Burakov, T. Geisler, C.T. Walker, M.L. Grange, A.A. Nemchin, J. Berndt, R.O.C. Fonseca, P.D.W. Bottomley, R. Hasnaoui, Micro-analytical uranium isotope and chemical investigations of zircon crystals from the Chernobyl "lava" and their nuclear fuel inclusions, Journal of Nuclear Materials 439(1-3) (2013) 51-56.
[23] A.A. Shiryaev, I.E. Vlasova, B.E. Burakov, B.I. Ogorodnikov, V.O. Yapaskurt, A.A. Averin, A.V. Pakhnevich, Y.V. Zubavichus, Physico-chemical properties of Chernobyl lava and their destruction products, Progress in Nuclear Energy 92 (2016) 104-118.
[24] B.E. Burakov, Lava-like materials formed and solidified during Chernobyl accident, Comprehensive Nuclear Materials 2nd edition2020, pp. 525-539.
[25] A.A. Shiryaev, B.E. Burakov, I.E. Vlasova, M.S. Nickolsky, A.A. Averin, A.V. Pakhnevich, Study of mineral grains extracted from the Chernobyl "lava", Mineralogy and Petrology 114 (2020) 489-499.
[26] TEPCO, Status of Fuel Debris Retrieval, 2021. https://www.tepco.co.jp/en/hd/decommission/progress/retrieval/index-e.html. (Accessed 29 March 2021).
[27] T. Kitagaki, K. Yano, H. Ogino, T. Washiya, Thermodynamic evaluation of the solidification phase of molten core–concrete under estimated Fukushima Daiichi nuclear power plant accident conditions, Journal of Nuclear Materials 486 (2017) 206-215.
[28] J.M. Hanchar, C.F. Miller, Zircon zonation patterns as revealed by cathodoluminescence and backscattered electron images: Implications for interpretaion of complex crustal histories, Chemical Geology 110 (1993) 1-13.
[29] S.L. Harley, N.M. Kelly, Zircon tiny but timely, Elements 3 (2007) 13-18.
[30] R.C. Ewing, W. Lutze, W.J. Weber, Zircon: A host-phase for the disposal of weapons plutonium, Journal of Materials Research 10(2) (2011) 243-246.
[31] R.V. Gentry, T.J. Sworski, H.S. McKnown, D.H. Smith, R.E. Eby, W.H. Christie, Differential lead retention in zircons: Implications for nuclear waste containment, Science, American Association for the Advancement of Science, 1982, pp. 296-298.
[32] B.E. Burakov, E.B. Anderson, V.S. Rovsha, S.V. Ushakov, R.C. Ewing, W. Lutze, W.J. Weber, Synthesis of zircon for immobilization of actinides, Scientific Basis for Nuclear Waste Management XIX, Material Research Society, 1996, pp. 33-39.
[33] T. Geisler, B. Burakov, M. Yagovkina, V. Garbuzov, M. Zamoryanskaya, V. Zirlin, L. Nikolaeva, Structural recovery of self-irradiated natural and ^{238}Pu-doped zircon in an acidic solution at 175°C, Journal of Nuclear Materials 336(1) (2005) 22-30.
[34] B.E. Burakov, M.I. Ojovan, W.E. Lee, Crystalline materials for actinide immobilisation, Imperial College Press2011.

[35] B.E. Burakov, E.B. Anderson, M.V. Zamoryanskaya, M.A. Yagovkina, E.E. Strykanova, E.V. Nikolaeva, Synthesis and Study of ^{239}Pu-Doped Ceramics Based on zircon, (Zr,Pu)SiO_4, and hafnon, (Hf,Pu)SiO_4, International Symposium on the Scientific Basis for Nuclear Waste Management XXIV, Material Research Society, Sydney, Australia, 2000, pp. 307-301.
[36] T. Geisler, U. Schaltegger, F. Tomaschek, Re-equilibration of zircon in aqueous fluids and melts, Elements 3 (2007) 43-50.
[37] D. Rubatto, O. Muntener, A. Barnhoorn, C. Gregory, Dissolution-reprecipitation of zircon at low-temperature, high-pressure conditions (Lanzo Massif, Italy), American Mineralogist 93(10) (2008) 1519-1529.
[38] T. Geisler, M. Zhang, E.K.H. Salje, Recrystallization of almost fully amorphous zircon under hydrothermal conditions: An infrared spectroscopic study, Journal of Nuclear Materials 320(3) (2003) 280-291.
[39] D. Bernini, A. Audétat, D. Dolejš, H. Keppler, Zircon solubility in aqueous fluids at high temperatures and pressures, Geochimica et Cosmochimica Acta 119 (2013) 178-187.
[40] A.E.S. Van Driessche, J.M. Garcia-Ruiz, K. Tsukamoto, L.D. Patiño-Lopez, H. Satoh, Ultraslow growth rates of giant gypsum crystals, Proceedings of the National Academy of Sciences of the United States of America 108(38) (2011) 15721-15726.
[41] S. Ueta, H. Satoh, Y. Nishimura, A. Ueda, K. Tsukamoto, Dynamic and topographic observation of calcite dissolution using enhanced in-situ phase-shift interferometry, Journal of Crystal Growth 363 (2013) 294-299.
[42] L. Nasdala, A.K. Kennedy, J.W. Valley, T.s. Váczi, P.W. Reiners, Sri Lankan gem zircon as reference material in analysis and research, Proceedings to 29th Technical Sessions of Geological Society of Sri Lanka, 2013, pp. 65-68.
[43] A.C. Lasaga., A. Luttge., Variation of crystal dissolution rate based on a dissolution stepwave model, Science 291 (2001) 2400-2404.
[44] M. Maruyama, K. Tsukamoto, G. Sazaki, Y. Nishimura, P.G. Vekilov, Chiral and achiral mechanisms of regulation of calcite crystallization, Crystal Growth & Design 9(1) (2008) 127-135.
[45] H.E. KIng, S. Hisao, T. Katsuo, P. Andrew, Surface-specific measurements of olivine dissolution by phases-shift interferometry, American Mineralogist 99 (2014) 377-386.
[46] H. Peter, Current knowledge on core degradation phenomena, a review, Journal of Nuclear Materials 270 (1999) 194-211.
[47] C. Journeau, P. Piluso, Core concrete interaction, Comprehensive Nuclear Materials2012, pp. 635-654.
[48] D.W. Akers, E.R. Carlson, B.A. Cook, S.A. Ploger, J.O. Carlson, TMI-2 core debris grab samples examination and analysis Part 1, Idaho Falls, 1986.
[49] D.W. Akers, E.R. Carlson, B.A. Cook, S.A. Ploger, J.O. Carlson, TMI-2 core debris grab samples examination and analysis part 2, Idaho Falls, 1986.
[50] D.J. Wronkiewicz, J.K. Bates, S.F. Wolf, E.C. Buck, Ten-year results from unsaturated drip tests with UO_2 at 90°C: Implications for the corrosion of spent nuclear fuel, Journal of Nuclear Materials 238 (1996) 78-95.

Table 1. Refractive index of each solution at 25°C

Solution	Refractive index, n_{25}
Ultra-pure water	1.332501
1 M HCl	1.341094
1 M NaOH aq	1.342259

Table 2. Properties of zircon

Mineral	Zircon
Locality	Ratnapura, Sri Lanka
Formula	$ZrSiO_4$
Formula weight	183.3071 g/mol
Density	4.85 g/cm^3
Crystal system and d-space	Tetragonal a = 6.604, b = 5.979, d_{101} = 4.432 Å

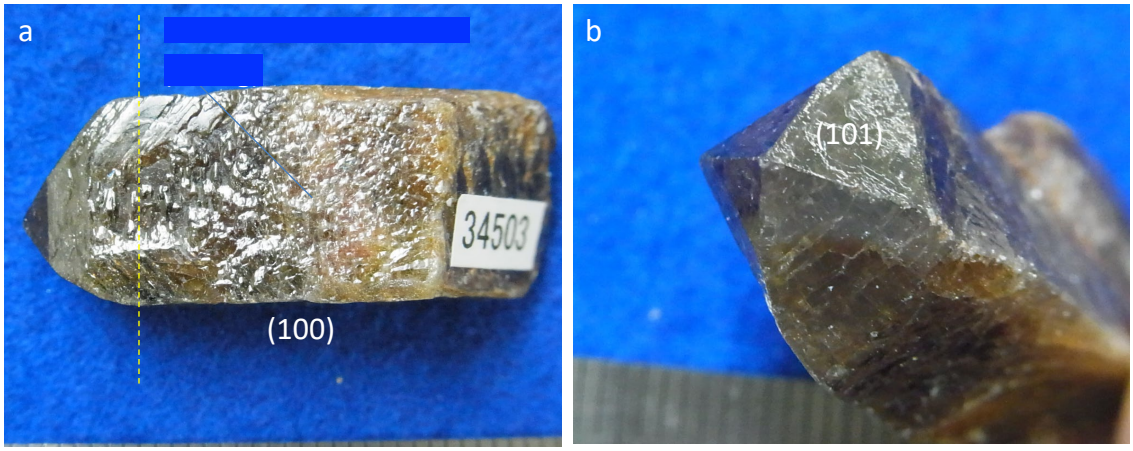

Figure 1. Zircon from Sri Lanka used in this experiment (a: (100) plane; b: (101) plane)

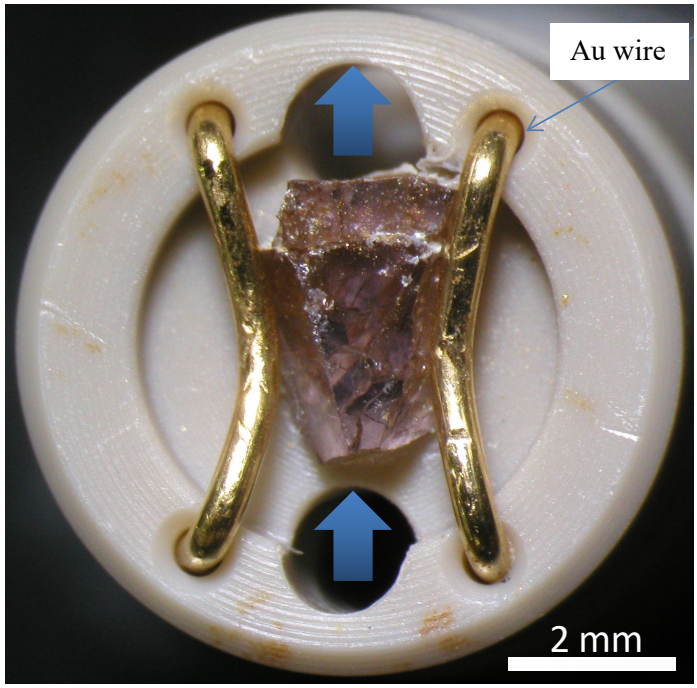

Figure 2. Zircon specimen fixed on the in situ observation cell

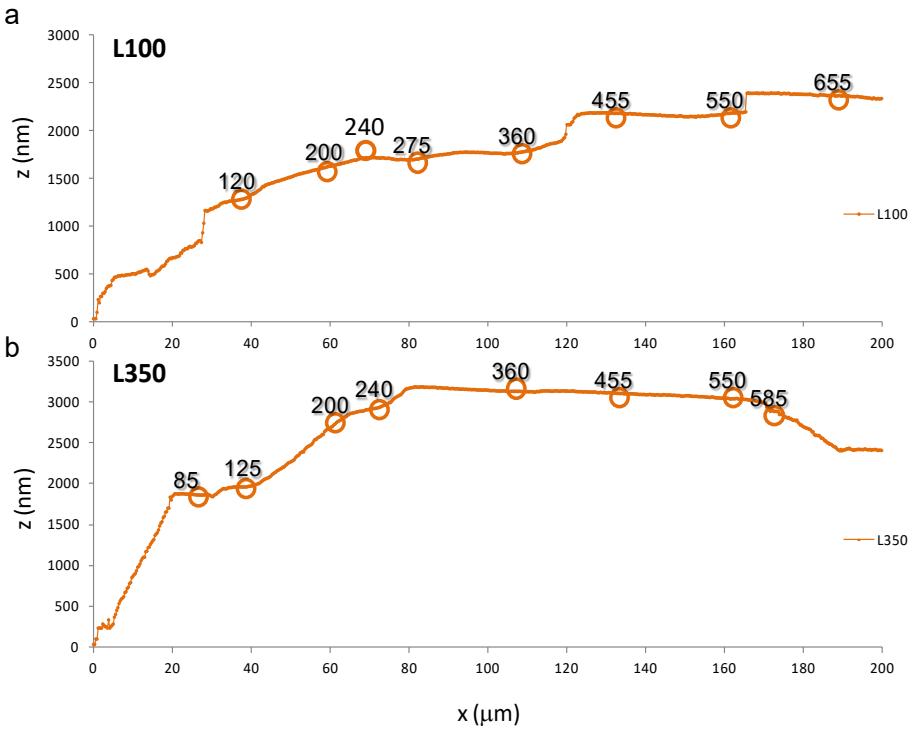

Figure 3. Height profile of L100 and L350 on the (101) plane of zircon during the flow of ultrapure water measured by HR-PSI

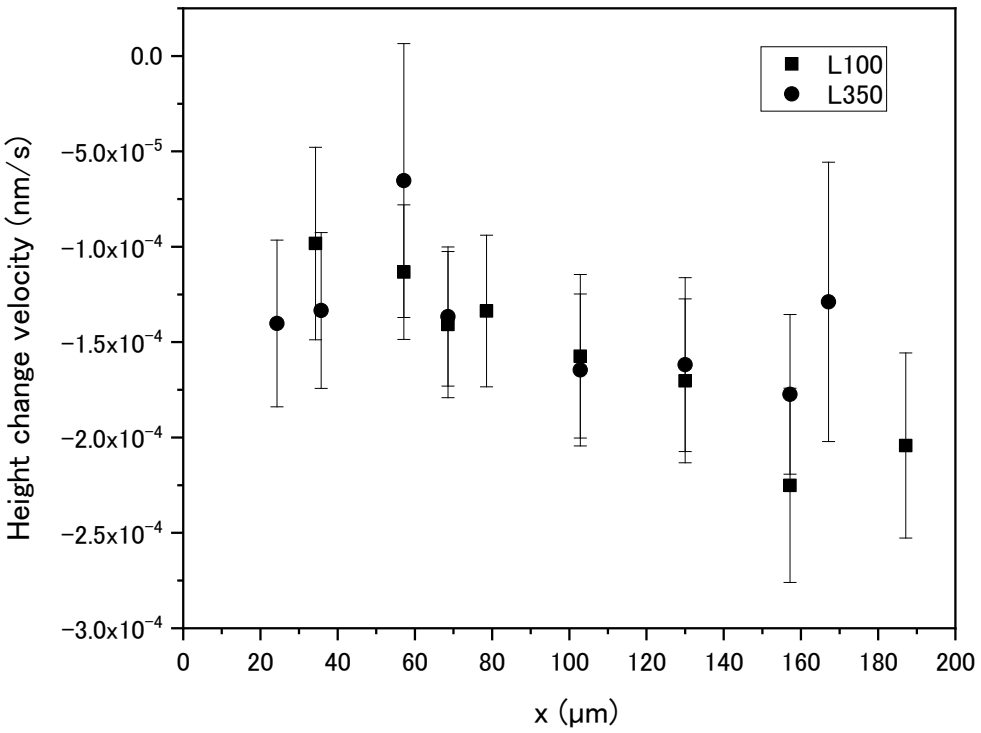

Figure 4. Height change velocity at each point on the (101) plane of zircon while flowing ultrapure water (Error bars show the standard error)

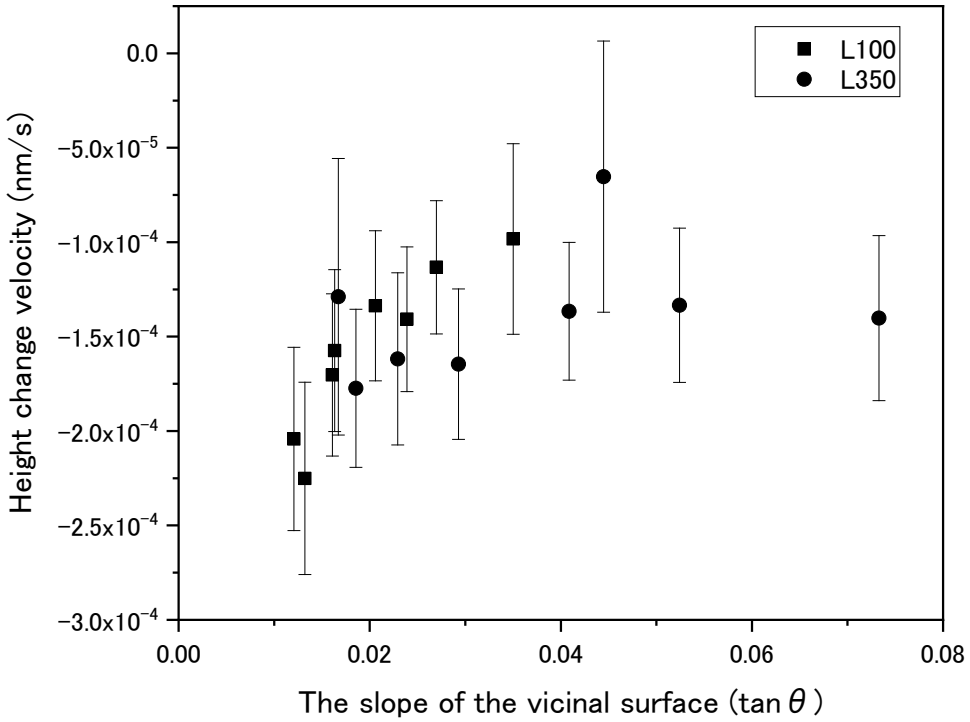

Figure 5. Height change velocity of ultrapure water dependent on the slope (Error bars show the standard error)

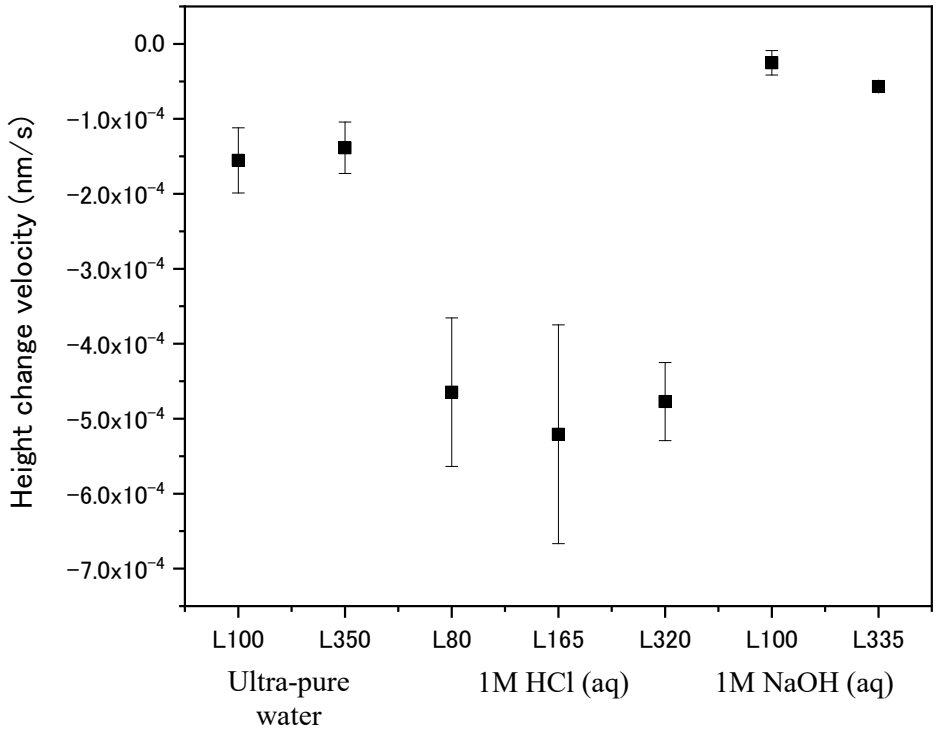

Figure 6. Height change of the lines on the (101) plane of zircon (Error bars show the standard deviation)

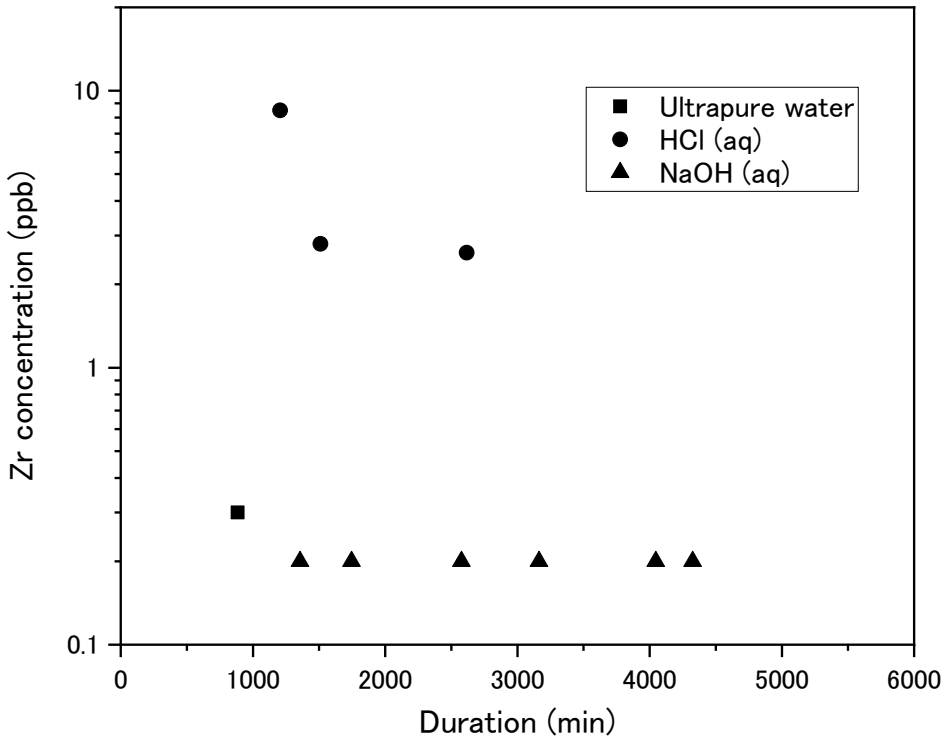

Figure 7. Change in Zr concentration in each solution with time

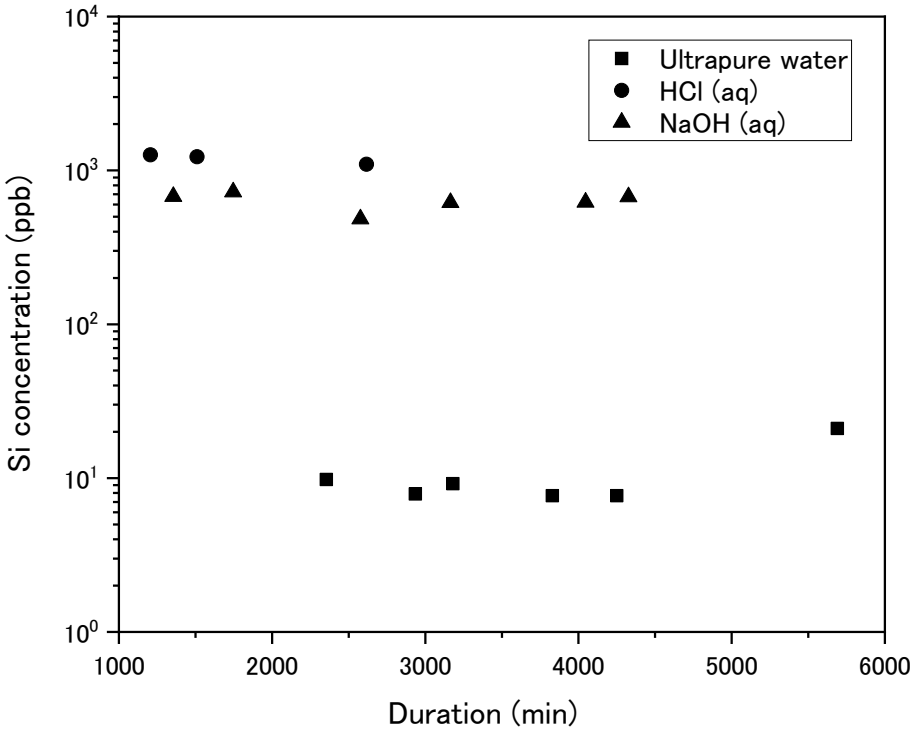

Figure 8. Change in Si concentration in each solution with time

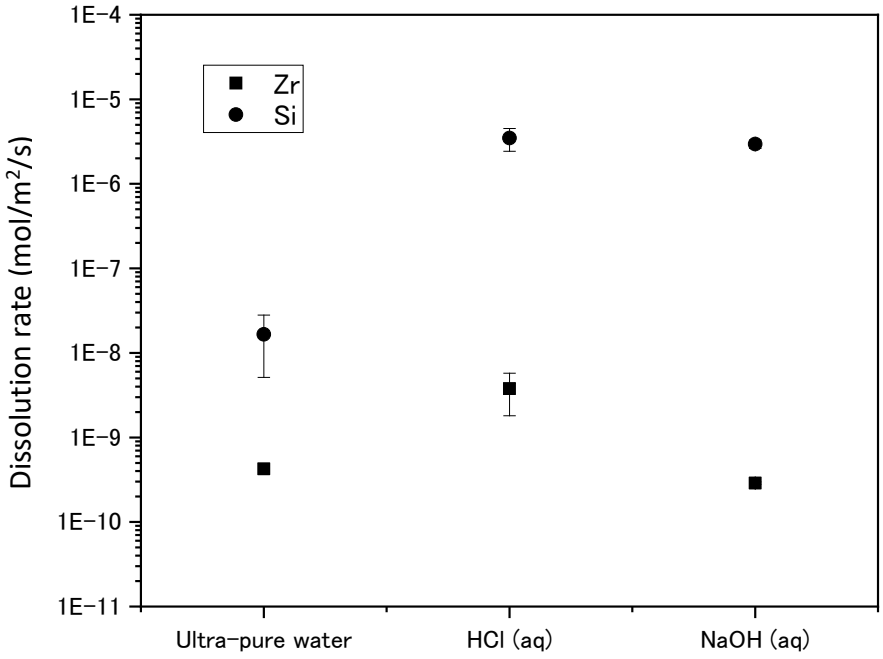

Figure 9. Dissolution rate of Zr and Si (Error bars show the standard deviation)

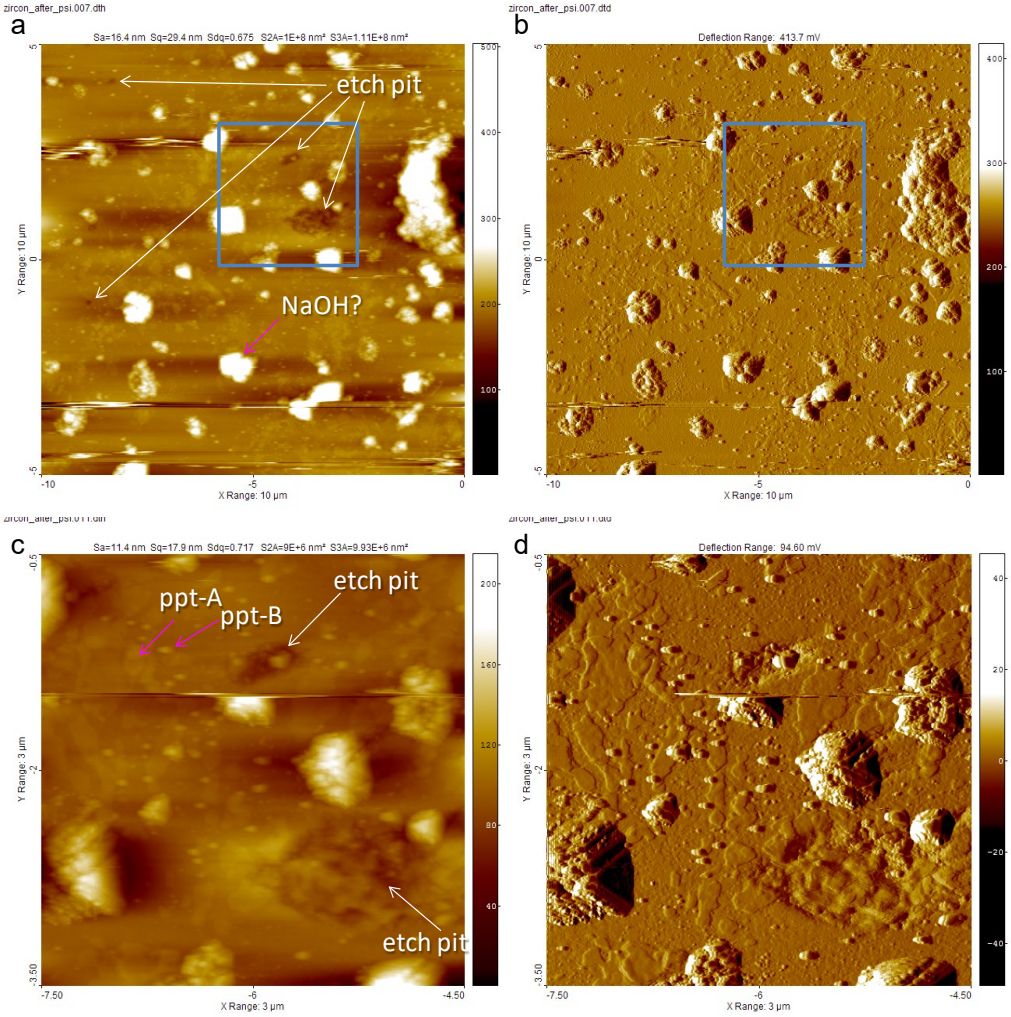

Figure 10. Surface of zircon after the HR-PSI measurements observed by AFM (a: 10 x 10 µm^2 surface height image; b: Derivative image of a; c: 3×3 µm^2 surface height image of the square in a; d: Derivative image of (c)